ELSEVIER

Chemical Engineering Journal 69 (1998) 53–61

Chemical Engineering Journal

# Crossflow microfiltration of shear-thinning aqueous titanium dioxide dispersions

P. Mikulášek [a,*], R.J. Wakeman [b], J.Q. Marchant [b]

[a] *Department of Chemical Engineering, University of Pardubice, nám. Čs. legií 565, 532 10 Pardubice, Czech Republic*

[b] *Department of Chemical Engineering, Loughborough University, Loughborough, Leicestershire, LE11 3TU, UK*

Received 4 June 1997; revised 22 October 1997; accepted 29 October 1997

**Abstract**

Crossflow microfiltration experiments were performed on aqueous dispersions of rutile (titanium dioxide) through a 0.1 μm pore size ceramic membrane at various operating parameters. The initial transient flux decline follows deadend filtration theory, with the membrane resistance determined from the initial flux and the cake resistance determined from the rate of flux decline due to cake build-up. For a long time, the observed fluxes reached steady or nearly steady-state values, presumably as a result of the cake growth being arrested by the shear exerted at its surface. The steady-state fluxes increase with increasing inlet crossflow velocity and decreasing feed concentration. The steady-state permeate flux values were determined from the steady-state model based on the Kozeny–Carman equation for cake resistance and Darcy's law applied over the filter area to relate filtration rate to average pressure difference between the feed and permeate sides of the filter. The model includes a cake resistance of the cake layer, which was determined for the titanium dioxide dispersions by fitting the experimental flux data to the model. The apparent viscosity of the dispersion, which is an input parameter in the flux model, is also adjusted to account for a model of the Herschel–Bulkley type. The resulting fluxes obtained from the model using simple values for the membrane resistance, cake resistance, and rheological parameters for each data set are in good agreement with the measured fluxes. © 1998 Elsevier Science S.A.

*Keywords:* Crossflow microfiltration; Titanium dioxide dispersion; Ceramic membrane

## 1. Introduction

Crossflow membrane microfiltration is a separation process for the removal of dispersed matters in sizes ranging from 0.05 to 10 μm from a liquid stream by forcing the liquid through a porous membrane. As opposed to deadend microfiltration, where the dispersion flow is normal to the membrane, the dispersion flows in crossflow filtration tangentially to the membrane surface. The tangential flow generates forces which tend to remove the deposited layers from the membrane surface thus, helping to keep the membrane relatively clean. The main applications of this process are in the production of ultrapure water, the processing of food and dairy products, the recovery of electrodeposition paints, the treatment of oil and latex emulsions and in biotechnology, oriented applications such as fractionation of fermentation broths and high performance reactors for enzymatic and fermentation processes. As well as solid–liquid separation processes, crossflow microfiltration of dispersions is encountered in a variety of other engineering applications such as wellbore drilling operations. The primary focus of our study is the crossflow microfiltration of concentrated dispersions of titanium dioxide in water. These concentrated dispersions arise in various industrial applications such as paints, coatings, and joint treatment compounds. These systems typically exhibit complex rheological behaviour [1,2].

Crossflow microfiltration can be operated on a continuous basis because the flow on the retentate side of the filter exerts a shear at the membrane surface. This shear prevents the continued build-up of a fouling or cake layer on the membrane surface, and a steady or quasi-steady permeate flux which often increases with the shear rate is observed. The mechanisms responsible for the steady-state reached in crossflow filtration processes are not clearly understood. Brownian diffusion is one likely mechanism for particles less than 0.1 μm diameter [3]. For larger particles, several possible mechanisms may be responsible for the steady-state. These include back-transport mechanisms such as inertial lift [4,5] and shear-induced diffusion [6–11] which carry particles away from the membrane, and surface-transport mechanisms [12] by which the shear forces and torques on a

* Corresponding author. Tel.: +420-40-582147; fax: +420-40-514530; e-mail: Petr.Mikulasek@upce.cz


*PII* S1385-8947(97)00108-3

particle at the cake surface overcome contact and adhesive forces. There are several reviews to which the interested reader may wish to refer [13–15].

In the present article, crossflow filtration experiments have been performed on aqueous dispersions of titanium dioxide through a tubular ceramic membrane. The feed concentration, flow rate and transmembrane pressure were varied. The focus is on determining the transient flux decline due to formation of a cake layer of rejected titania particles and the steady-state flux due to shear forces arresting the growth of the particle cake. The approximate procedure to predict the total behaviour of the permeate flux, from time zero to steady-state, is to use the deadend filtration theory until the time the steady-state is reached and then use the steady-state flux value from the steady-state model based on cake theory which applies Darcy's law to relate filtration rate to the average pressure difference between the feed and permeate sides of the filter. The goal is to obtain a better qualitative and quantitative understanding of the factors affecting titania dispersion filtration under crossflow conditions.

## 2. Experimental

### 2.1. Materials

The titanium dioxide used was rutile supplied by Tioxide Group, England. Rutile (density: 4260 kg $m^{-3}$) has a higher refractive index, higher density and greater chemical stability than anatase. The crystal size for rutile $TiO_2$ pigments, which is distinct from particle size (0.25–0.40 $\mu$m), is 0.17–0.24 $\mu$m. Transmission electron microscopy was used to estimate the shape and aspect ratio of the rutile crystals, which were found to be approximately elliptic and 2–3, respectively. The particle size distributions were measured using a MasterSizer MS20 (Malvern Instruments, England).

The dispersions were prepared by mixing the appropriate amount of 'Millipore-filtered' water and titanium dioxide in a high shear Ultra-Turrax T25 mixer (Janke & Kunkel, IKA-Labortechnik, Germany) using CALGON (sodium hexametaphosphate) as a dispersant. The samples were prepared containing 0.15% by weight of dispersant. Even as the volume percent of solids was varied, the mass of dispersant per unit mass of solids was kept unchanged. This was to ensure that there was always an adequate amount of dispersant available for steric stabilisation.

Zeta potential measurements to get information on the state of the charge at the solid–liquid interface were carried using a microelectrophoresis device (Zetasizer 3, Malvern Instruments, England).

The pH level of the system was adjusted to pH 9 with 0.05 M analytical grade NaOH in deionised water, which was used as the suspending medium. The pH was measured with a Model 80 (Griffin & George, England) pH meter. The dispersion was stirred until a steady pH reading was obtained. At pH 9 the zeta potential was about $-50$ mV enabling a stable, well dispersed suspension to produced.

### 2.2. Rheological measurements

A Carri-Med Model CS 100 controlled stress rheometer, with either a double concentric or a cone and plate system, was used for the steady shear measurements. The cone and plate system was used only for the highest volumetric concentrations of solids in the samples (50 vol.%). The temperature of the samples was controlled by a Peltier system. All measurements except those of the temperature effect study were conducted under ambient conditions ($T = 20$°C). Measurements of the effect of temperature were conducted for temperatures ranging from ambient to 50°C. The temperature was maintained to within $\pm 0.1$°C of the desired preset value. Water evaporation was potentially a serious problem when the experiment was performed above 30°C. Therefore, the interface exposed to the atmosphere was coated with a thin layer of silicone oil to minimise evaporation. The rheological measurements suggested the use of a model of the Herschel–Bulkley type

$$\tau = \tau_{HB} + K\dot{\gamma}^{n} \quad (1)$$

or of the Casson type

$$\tau^{1/2} = \tau_C^{1/2} + (\eta_\infty \dot{\gamma})^{1/2} \quad (2)$$

to characterise the rheological behaviour of these dispersions [16]. The existence of a yield stress has been observed, especially at the highest volumetric concentrations of solids. In addition, it should be noted that a positive value for the hysteresis loop area has been obtained and this indicates that the samples with the highest concentrations of the solids had some thixotropy.

### 2.3. Filtration experiments

#### 2.3.1. Membranes

The ceramic membranes studied in this work were asymmetric, double-layered, silicon carbide (SiC) membranes (Atech Innovations, Germany). They were configured as single cylindrical tubes 0.9 m long, 16 mm ID and 25 mm OD, consisting of a thin SiC layer deposited on the internal surface of the tubular support. In our experiments, the microfiltration membranes were used with the mean pore diameter of 0.1 $\mu$m.

#### 2.3.2. Equipment

A schematic diagram of the experimental apparatus is shown in Fig. 1. The dispersion is fed to the filter by a variable speed Mono pump, thus allowing a range of crossflow velocities to be examined. Pressure transducers at either end of the filter module measure the transmembrane pressure, which is controlled using full flow ball valves. Temperatures are monitored by thermocouples, computer controlled, and maintained by a hot water jacket around the feed tank. An auto-

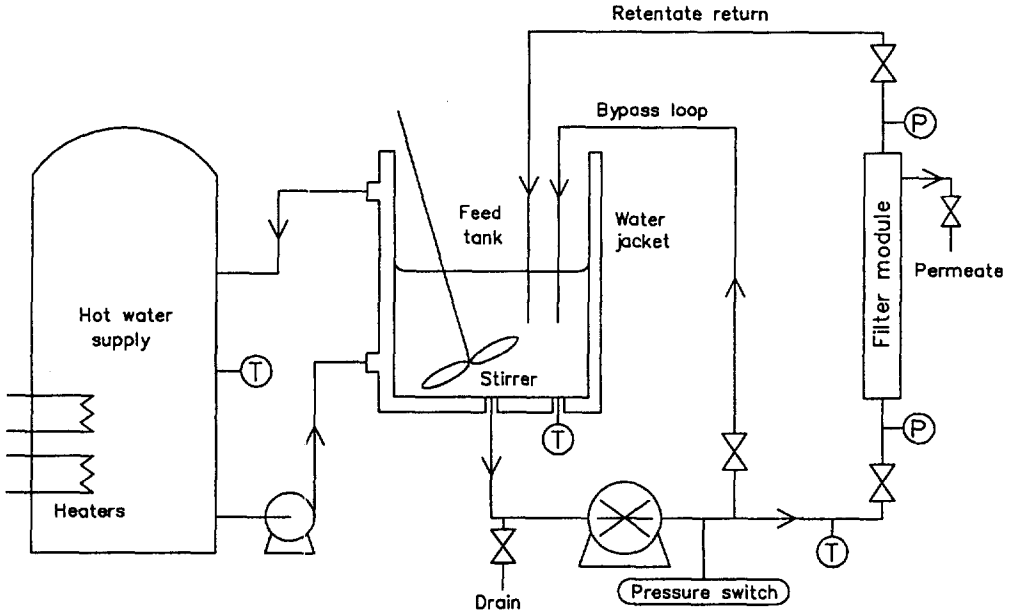


Fig. 1. Schematic diagram of crossflow microfiltration rig.

matic data logging system records transmembrane pressure, temperature and pump speed while permeate flux measurements are taken manually.

Once the dispersion is circulating through the bypass loop at the required volumetric flow rate, concentration, pH, and temperature, the valve to the filter module is opened and the bypass loop closed. The filter module exit valve is then adjusted to achieve the desired transmembrane pressure, following which permeate flux readings are taken and the flux decline monitored until a steady-state is reached.

Experiments were carried out at 50°C. The permeate flux, $J$, for various inlet crossflow velocities in the range 0.3–2 m $s^{-1}$ and various transmembrane pressures in the range 50–200 kPa, was evaluated. The same membrane was used in each experiment, and before the run, the pure water flux through the membrane was measured. The flux through the membrane was measured by collecting the permeate from the outer stainless steel tube surrounding the membrane into a graduated cylinder and timing the collection period. Both the permeate and the retentate were recycled to the storage tank. Therefore, the concentration in the container remained effectively constant. The unit allowed studies in which the transmembrane pressure and the crossflow velocity were independently varied. By systematically adjusting one process variable while maintaining all others constant, steady-state permeate flux values were obtained as a function of each variable.

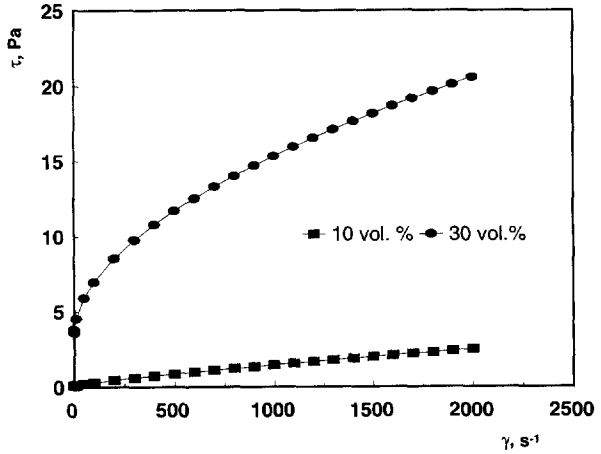


Fig. 2. Rheogram of the shear stress against the shear rate for 10 and 30 vol.% titanium dioxide dispersions at pH 9 and temperature 50°C.

Table 1
Parameters of the Herschel–Bulkley model as a function of the solids volume fraction of aqueous titania dispersions ($T = 50$°C)

| $\phi$ | $\tau_{HB}$ [Pa] | $K$ [Pa $s^n$] | $n$ |
|---|---|---|---|
| 0 | 0 | $5.494 \times 10^{-4}$ | 1 |
| 0.05 | 0.0106 | $1.519 \times 10^{-3}$ | 0.919 |
| 0.10 | 0.1592 | $4.468 \times 10^{-3}$ | 0.834 |
| 0.20 | 1.459 | 0.1041 | 0.676 |
| 0.30 | 3.517 | 0.2982 | 0.529 |
| 0.40 | 10.99 | 0.6232 | 0.487 |
| 0.50 | 25.52 | 1.108 | 0.448 |

## 3. Results and discussion

### 3.1. Viscosity measurements

The results of the viscosity measurements are presented in Fig. 2 showing a pronounced non-Newtonian behaviour of the aqueous titania dispersions (in agreement with data presented in Ref. [2]). The pronounced shear-thinning rheological behaviour can be approximated with a model of the Herschel–Bulkley type or of the Casson type. For the former, Table 1 gives the values obtained for the various parameters as functions of the solids volume fraction.

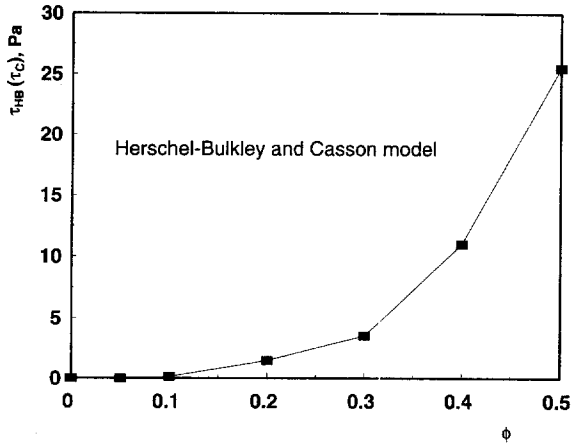


Fig. 3. Variation of the yield stress as a function of the solids volume fraction.

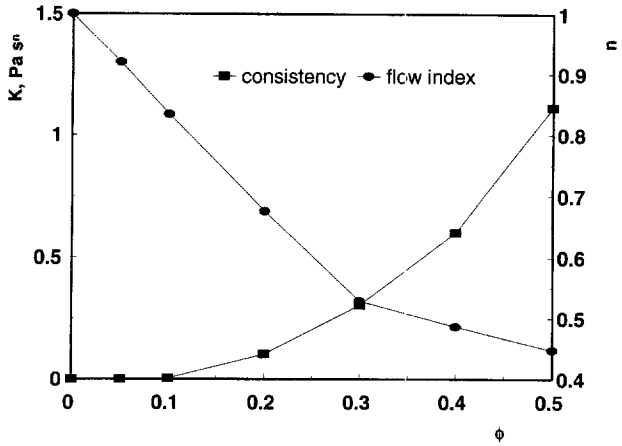


Fig. 4. Variation of the consistency and the flow index as a function of the solids volume fraction (Herschel–Bulkley model).

A plot of the variation of the yield stress as a function of the solids volume fraction (see Fig. 3) shows that neither $\tau_{HB}$ or $\tau_C$ increases strongly above concentration of 10%. The values of the yield stresses, calculated on the basis of the two rheological models, are very close to one another for the volume fractions above 10% (the differences between the two values fall between 2 and 5%). The percentile difference is considerably larger for lower concentration.

The consistency, $K$, of the Herschel–Bulkley model (see Fig. 4) also increases strongly above this critical volume fraction of 10%. In addition, in this same figure, the curve for the variation of the flow index, $n$, of the dispersion shows clearly that there is a change in the rheological behaviour of the titania dispersions when the solids volume fraction exceeds 30%. For the Herschel–Bulkley model, the variation of the yield stress, consistency, and of the flow index, can be represented by the relationships

$$\tau_{HB} = 235\phi^{3.275} \quad (3)$$

$$K = 5.494 \times 10^{-4}(1-\phi)^{-19.93} \text{ for } \phi \leq 0.1 \quad (4a)$$

$$K = 6.564\phi^{2.573} \text{ for } \phi > 0.1 \quad (4b)$$

$$n = 1 - 1.574\phi \text{ for } \phi < 0.3 \quad (5a)$$

$$n = 0.65 - 0.405\phi \text{ for } \phi > 0.3 \quad (5b)$$

The empirical relationships presented in Eqs. (3), (4) and (5) are based on experimental measurements over a concentration range $0 < \phi < 0.5$, and are expected to be valid during crossflow microfiltration of these dispersions.

### 3.2. Typical flux decline curves

Analysis of the permeate composition showed complete retention of the titania particles in the feed. Note that no long term flux decline was observed, which is not surprising since the particles were bigger than the membrane pores.

The expected dependence of crossflow microfiltration behaviour on dispersion stability (or pH) in the case of titania-in-water dispersions has been shown experimentally [17]. In contrast to the case studied in this paper, the unstable dispersion (pH 4) shows different filtration characteristics. The different qualitative behaviour could be explained by the formation of very large flocs in the case of the unstable dispersion [2].

The effect of inlet crossflow velocity, $u$, and bulk dispersion solids volume fraction, $\phi$, on the permeate flux-time curve are depicted in Figs. 5 and 6. As a general rule, the steady-state flux during crossflow microfiltration was sub-

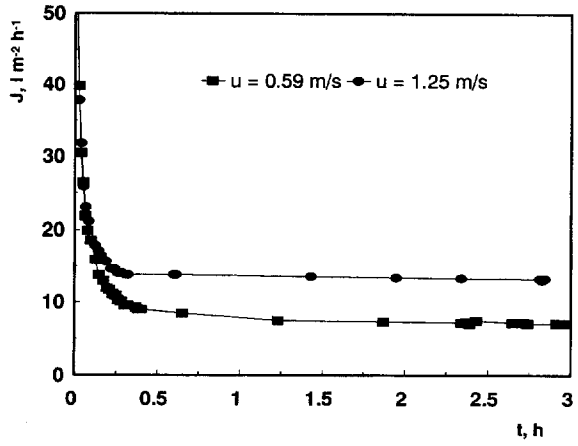


Fig. 5. Effect of inlet velocity on flux-time curve ($\phi = 0.19$, $\Delta P = 100$ kPa).

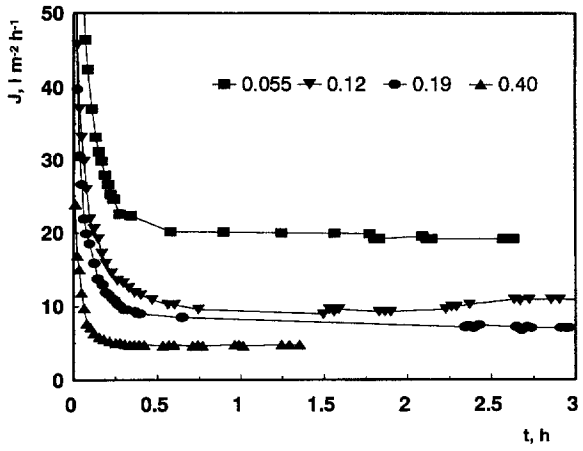


Fig. 6. Effect of bulk solids volume fraction on flux-time curve ($u = 0.7$ m s$^{-1}$, $\Delta P = 100$ kPa).

stantially lower than the pure water flux ranging from 1% to 10% of the pure water values. Besides the fact that low levels of permeate flux were achieved (for comparison see Refs. [18,19]), the most noticeable feature in Figs. 5 and 6 is the strong dependence of the flux on the operating variables. The following trends are evident: (a) a significant flux decay was observed mainly in the initial periods of the process, and (b) the flux decline shows significant dependence on operating conditions such as inlet velocity and bulk dispersion solids volume fraction.

The flux decay in the initial periods of the process could be explained by build-up of a cake layer on the membrane surface which offers the controlling hydraulic resistance to permeation. Steady-state conditions are reached when the convective transport of particles to the membrane is equal to the sum of the permeate flow plus the diffusive back transport of the particles. In addition, the filter cake continues to grow until it reaches a state where further growth is curtailed by the applied axial fluid shear upon the cake layer. At this point, a steady-state flux should be reached.

The effects of the operating variables on the steady-state flux are shown in Fig. 7. The steady-state flux is a strong function of the operating variables investigated. It is evident from Fig. 7 that the steady-state flux increases (the thickness of the cake layer and its hydraulic resistance decreases) with the superficial velocity. Similar trends were observed before [18,20–22]. Increasing the crossflow velocity of the dispersion increases the shear effect on the filter cake surface. This helps to limit the thickness of filter cake formed, but may also serve to agitate particles in the cake surface layer, resulting in cake consolidation and therefore, an increased resistance to permeate flow [23].

The effects of increasing dispersion concentration on permeate flux can be seen in Fig. 7. At higher concentrations, the relatively high initial flux of particles to the filter surface results in the rapid deposition of a cake layer, minimising the tendencies of particle penetration into the membrane pores and resulting in a more immediate decline in permeate flux. At steady-state, the higher concentration results in a thicker filter cake and consequently a lower permeate flux. Additionally, the effects of pH, crossflow velocity and transmembrane pressure on permeate flux are all more pronounced at low concentrations and have reduced effect at higher concentrations [17]. At pH 4, close to the isoelectric point, the permeate flux is much higher than at other pH values. For example, the steady-state flux when filtering a 4% by volume feed is about 380 l $m^{-2}$ $h^{-1}$ at pH 4 and 30 l $m^{-2}$ $h^{-1}$ at pH 9.5. With a 12% feed the corresponding fluxes are 130 and 20 l $m^{-2}$ $h^{-1}$ (these fluxes were all measured at a transmembrane pressure of 100 kPa, crossflow velocity of 1.3 m $s^{-1}$ and temperature of 50°C). Increasing the transmembrane pressure increased the steady-state permeate flux; for example, filtering 33% feed (using a crossflow velocity of 0.8 m $s^{-1}$, pH 9.5, 50°C) produced fluxes of 3.3, 4.7 and 6.5 l $m^{-2}$ $h^{-1}$ at transmembrane pressure of 50, 100 and 200 kPa. The highest concentration reached during filtration was 48% solids by volume (pH 9.5, 50°C, 100 kPa, 1.3 m $s^{-1}$).

Of interest is the semi-log relationship exhibited between steady-state permeate flux and log volume solids fraction (Fig. 8), a trend also observed by Fane [24]. Such linear relationships have been found when filtering other dispersed systems; by extrapolating the permeate flux ($J_{ss}$) vs. log[feed concentration ($\phi$)] to obtain a concentration that corresponds to $J_{ss}=0$, a so-called gel concentration ($\phi_g$) can be defined—more correctly referred to as a cake concentration in this work. Fig. 8 indicates that $\phi_g$ is independent of the filter operating conditions; this has also been found from the crossflow filtration of surfactant [25–27] and latex [28] dispersions, water soluble polymers [29] and for filtering some proteins under certain conditions [30]. However, $\phi_g$ does depend on the solute (particle)-membrane interactions [31].

Clearly, the effects that operating variables have on flux differ from system to system. The only general conclusion that may be drawn is that the permeate flux increases with operating velocity and decreases with increasing dispersion concentration. This probably explains why models developed for a particular system may often contradict experimental

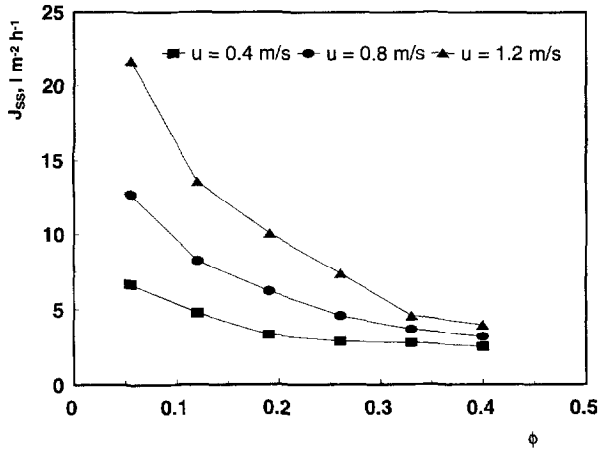


Fig. 7. Effect of crossflow velocity and bulk solids volume fraction on the steady state flux.

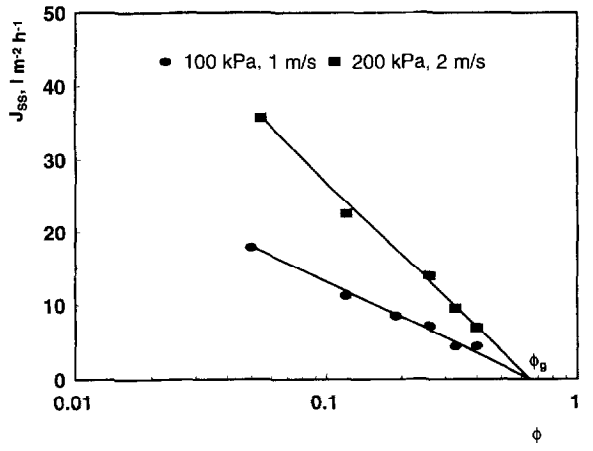


Fig. 8. Semi-log relationship between the steady state flux and bulk solids volume fraction.

observations obtained on different systems (see, for example, Refs. [13–15]).

### 3.3. Comparison of experiments with theory

The general trends predicted by the theory presented in the previously published papers [13–15]—such as an increasing permeation flux with increasing transmembrane pressure difference and shear rate, and a decreasing permeation flux with increasing feed volume fraction—have been verified experimentally.

Crossflow filtration limits the build-up of rejected particles on the membrane, and at steady-state the particle layer formed on the walls is assumed to attain a thickness that is invariant with time but increases with axial distance from the filter entrance. The resistance produced by the cake and flowing (polarised) particle layers along with the intrinsic resistance of the membrane are considered to act in series, and the permeate flux is then described by Darcy's law. The resistance due to the flowing layer is usually much less than the membrane resistance and is inconsequential in all cases of practical interest [9]. Thus

$$J_{ss} = \Delta P/\mu_o(R_m + r\delta) = J_o R_m/(R_m + r\delta) \quad (6)$$

where $J_{ss}$ is the steady-state permeate flux, $\mu_o$ is the solvent (in this case, water) viscosity, $R_m$ is the membrane resistance, $r$ is the cake resistance, and $\delta$ is the cake thickness. The second equality in Eq. (6) expresses $J_{ss}$ as a function of the permeate flux of the clean membrane: $J_o = \Delta P/\mu_o R_m$. The resistance of the cake layer, $r$, is estimated using the Blake–Kozeny correlation [32]

$$r = 37.5\phi_{max}^2/a^2(1-\phi_{max})^3 \quad (7)$$

where $\phi_{max}$ = volume fraction of the maximally packed particles in the cake layer.

#### 3.3.1. Analysis method for time-dependent permeate flux

The effect of time-dependent decreases in permeate flux on the average permeate flux over an operating time, $t$, can be approximated using a procedure in which the steady-state model for crossflow filtration is combined with a transient model for deadend batch filtration. This procedure has been shown [13,14] to yield a good approximation to the exact solution [11] for the time varying permeate flux $J(t)$. A mathematical analysis of the classic constant pressure blocking filtration laws, with due allowance for a crossflow removal mechanism, has been completed by Field et al. [33]. However, this work demonstrates that provided certain terms take finite values, fluxes should exist at which there is no decline of flux with time.

An explicit solution for $J(t)$ is derived from a mass balance at the edge of a growing cake layer in a deadend filtration operation [13]:

$$(J + d\delta/dt)\phi = \phi_{max} d\delta/dt \quad (8)$$

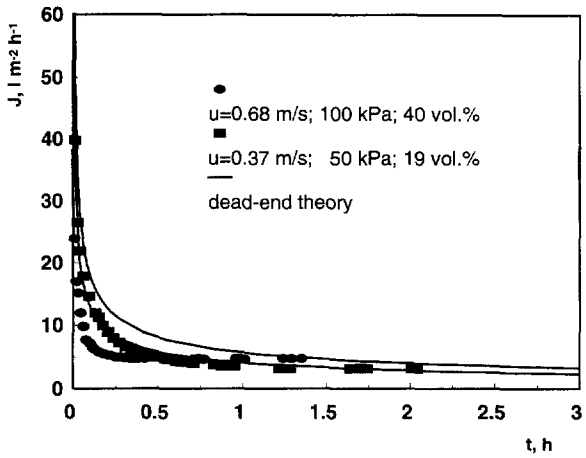


Fig. 9. Comparison between predicted and experimentally observed flux-time curves.

Eq. (8) is combined with Eq. (6) and integrated to give the following expression for the time-dependent permeate flux [14]:

$$J(t) = J_o/(1 + 2t/\tau_{cr})^{1/2} \quad (9)$$

where $\tau_{cr} = R_m(\phi_{max} - \phi)/(J_o r\phi)$ is the time constant associated with the flux decline.

The approximate procedure to predict the total behaviour of the permeate flux, from time zero to steady-state, is to use Eq. (9) from deadend batch filtration until the time the steady-state is reached and then use the steady-state flux value from the steady-state model [14]. The underlying reason behind this combined solution is that while the cake is initially developing, the effect of the shear rate is small and can be neglected over short times so that crossflow filtration theory can be effectively approximated by deadend filtration theory. Nearing the steady-state, however, the shear rate begins to arrest the cake growth in crossflow filtration while deadend flux profile continues to decline with time. The approximate time to steady-state, $t_{ss}$, is determined by substituting the steady-state flux, $J_{ss}$, in Eq. (9)

$$t_{ss} = [(J_o/J_{ss})^2 - 1]\tau_{cr}/2 \quad (10)$$

The characteristics of permeate flux decline, and the associated operating time required to achieve the steady-state flux, vary as a function of the concentration of dispersions and operating parameters.

The results for the permeate flux as a function of the time are shown in Fig. 9. The solid lines are the theoretical predictions for the conditions corresponding to those of the experiments. The quantitative agreement between theory and experiment is good, although the theory overpredicts the permeate flux observed in some of the experiments (see Fig. 9). This may indicate that the cake layer resistance determined from Eq. (7) was less than its value during microfiltration. Note that the transient flux decline follows the deadend theory given by Eq. (9) for short times and then levels off for long times.

*3.3.2. Analysis method for steady-state flux*

The steady-state thickness is found from a balance between the convective transport of particles toward the cake and the shear-induced transport or diffusion of particles away from or along the top of the cake. For an initially clean membrane, and unless the shear rate at the membrane surface exceeds a critical value, particles are convected to the membrane with the permeate flux more rapidly than they are removed. As a result, the stagnant cake layer forms and grows. The permeate flux is reduced as the cake thickness increases (due to increased cake resistance), and the shear at the cake surface increases as the cake thickness increases (due to reduced cross-sectional area for axial flow, and assuming that the feed pump is able to deliver a constant flow rate as the channel becomes constricted).

The model of Datta and Gaddis [34], using the Kozeny–Carman equation for cake resistance and Darcy's law applied over the filter area to calculate steady-state cake thickness or permeate flux was used. Mathematically, the limiting cake thickness may be obtained from the simultaneous solutions of the pressure drop due to Kozeny–Carman drag due to flow through a packed bed having uniform volume concentration of the cake, which is equal to the maximum packing density for the solids, $\phi_{max}$. Therefore, at steady-state the cake thickness can be predicted from Datta and Gaddis [34] as

$$(R_m\delta^2 + r\delta^3)\tau/\eta_c = [2\Delta P\phi/\mu_o(\phi_{max} - \phi)]x \quad (11)$$

where $\tau$ is the shear stress, $x$ is coordinate denoting longitudinal direction of feed (dispersion) flow, and $\eta_c$ is the cake apparent viscosity, which can be determined from Mooney's equation [35]

$$\eta_c/\mu_o = \exp[2.5\phi_{max}\phi^*/(\phi^* - \phi_{max})] \quad (12)$$

Here $\phi^*$ ($=0.74$) is the maximal value of the packing density (volume concentration) of rigid spheres [35].

It should be noted that the theoretical model requires values for volume fraction in the cake layer and apparent shear viscosity of bulk dispersion. The volume fraction of the maximally packed particles in the cake layer, $\phi_{rnax}$, was not measured directly, but a reasonable estimate is given by $\phi_g = \phi_{max} = 0.65$, from Fig. 8. Alternatively, it has been suggested that $\phi_{max}$ up to 0.65 can be used [28]. The apparent shear viscosity for the dispersion at different concentrations was determined from the data of Mikulášek et al. [2] by

$$\eta = \tau_{HB}/\gamma + K\gamma^{n-1} \quad (13)$$

Corresponding values of yield stress, $\tau_{HB}$, consistency, $K$, and flow index, $n$, Eqs. (3), (4) and (5) respectively, were used in Eq. (13).

From Eq. (11) the cake layer thickness distribution $\delta(x)$, (i.e., variation of the cake thickness with longitudinal distance, $x$) can be calculated. Model parameters required for the solution of the steady-state equation, i.e., the maximum solids volume fraction, $\phi_{max}$, the shear stress, $\tau$, and the cake layer resistance, $r$, were subsequently quantified on experimental data. A solution procedure was used (see Refs. [34,36]), enabling prediction of the steady-state cake thickness. This thickness (Eq. (11)) yields a distribution $J(x)$ whose average value is the observed mean steady-state, length-averaged permeate flux for specified operating variables. The cake thicknesses in the range from $1\times10^{-3}$ to $7.5\times10^{-3}$ m were estimated, which were in agreement with visual observation of the filter cake after microfiltration. At high feed concentration, the filter tube was almost blocked by cake.

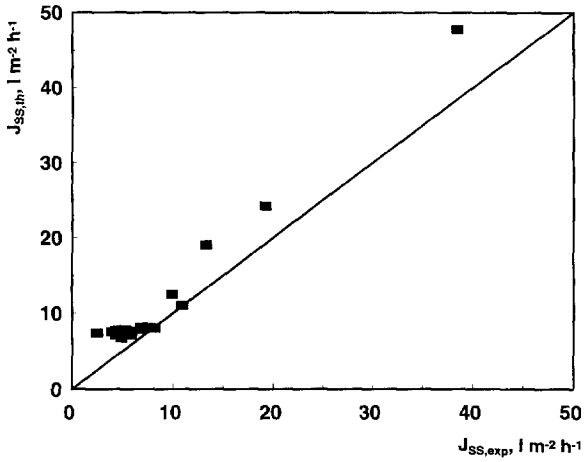


Fig. 10. Comparison between predicted and experimentally observed steady state fluxes ($\Delta P = 100$ kPa).

The overall model performance is shown in Fig. 10, where predicted steady-state fluxes are compared to experimental values. The quantitative agreement between theory and experiment is good, although the theory overpredicts the steady-state permeate flux observed in our experiments (Fig. 10). This may indicate that a flowing sublayer was present over the stagnant cake layer or that the apparent viscosity of the cake was somewhat lower than the value used in making the theoretical predictions and/or the cake layer resistance determined from Eq. (7) was less than its value during microfiltration. The apparent viscosity of the cake layer estimate is quite sensitive to the viscosity model used to correlate concentration with viscosity. Though Mooney's model (Eq. (12)) [35] may be adequate for high shear stresses it may underpredict the apparent viscosity values at smaller shear stresses. This inference can be drawn easily based on the experimental apparent viscosity values for titania dispersions [34].

Crossflow experiments were conducted to investigate the effects of module hydrodynamics and dispersions parameters on permeate flux. However, even though an increased shear decreased the mass of particles deposited, thinner cakes did not necessarily result in higher permeate fluxes in experiments using the more widely distributed particles and low initial permeation rates. Thus, the benefits of a decrease in the cake mass at higher shear rates (or shear stress) may be counteracted by an increase in the cake resistance. In other words, the cake resistance during the microfiltration of a polydisperse dispersion is dependent on operating conditions. This may be attributed to two phenomena:

1. higher shear stresses selected for smaller particles in the cake in these experiments, and
2. higher shear stresses may favour more dense packing geometries.

Hydrodynamic selection of smaller particles and cake reorganisation result in cakes with a higher resistance during the crossflow microfiltration of polydisperse dispersions [22]. Thus, increasing the wall shear stress beyond a critical value is expected to have a limited value in increasing permeate flux. Similar observations have also been made during the turbulent crossflow filtration of mineral suspensions that formed compressible cakes [37].

As the shear rate increases progressively, smaller particles in the feed are expected to be selectively deposited [38]. Cakes formed at higher shear rates are also expected to be more compact. Therefore, for a given composition of the feed (i.e., solids volume fraction, $\phi$) the cake resistance should increase with shear rate. Also, because initially deposited particles are less likely to be rearranged at higher permeation rates, cake resistance should be inversely related to $J_o$ for any given inlet crossflow velocity of bulk dispersion. Experimental data from the experiments are consistent with these expectations.

One way to estimate the cake resistance is to parameter fit the model prediction to the measured time dependent permeate flux. The graphs of $[(J_o/J)^2 - 1]$ vs. $t$ was plotted for the titania dispersions flux decline data. These graphs yield a straight lines for short times. This confirms that the transient flux decline occurs due to formation of a cake layer of the rejected particles, similar to deadend filtration. For longer times, the data deviate from the straight line. This is because the arrest of cake growth due to shear causes the flux for crossflow microfiltration to be greater than for the deadend filtration after the same time interval: hence, the value of $[(J_o/J)^2 - 1]$ becomes less for the crossflow mode as compared to deadend filtration at longer time intervals. A linear regression of the data was performed to give an equation for the best-fit line. From the slope of the line the cake resistance has been calculated. The cake resistances for the titania dispersions were determined on the order of $(2\text{–}4) \times 10^{16}\ m^{-2}$.

Fig. 11 illustrates the effect of taking the experimentally determined specific cake resistance into account in the calculation of permeate flux. In all these theoretical predictions, the respective values of the membrane resistance and the cake resistance cited above were used. The symbols are the measured fluxes, and the solid lines are the fluxes predicted by the deadend theory and by the steady-state model based on the Kozeny–Carman equation for cake resistance and Darcy's law applied over the filter area to relate filtration rate to average pressure difference between the feed and permeate sides of the filter. Tube constriction due to formation of thick cake layers is accounted for in the theoretical predictions.

Predicted fluxes show a notably good correspondence with experimental values. This is remarkable in view of the fact that correlations employed in the model were developed for systems vastly different from the crossflow microfiltration system used in this work. The filtration flux correlates well with wall shear stress, reducing to a unique relation in the absence of pore plugging, i.e., when the filter resistance is dominated by the properties of the deposit and flow conditions. Thus, the filter tube diameter and rheological properties of the dispersions will influence the wall shear stress and have a consequent effect on the flux.

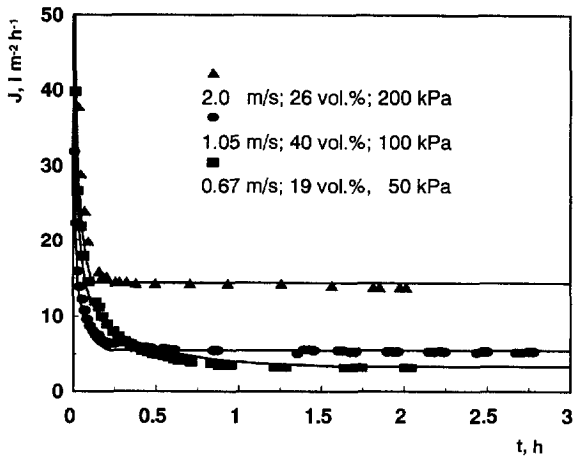


Fig. 11. Comparison between predicted and experimentally observed flux-time curves at different operating variables.

## 4. Conclusions

The characteristic permeate flux-time behaviour and effects of operating variables on flux data have been presented for aqueous titanium dioxide dispersions that were crossflow microfiltered in a ceramic membrane tube.

The flux-time curve, and the steady-state permeate flux, are functions of all the operating variables studied, i.e., inlet crossflow velocity of bulk dispersion, bulk solids volume fraction and transmembrane pressure difference.

The transient flux decline under crossflow conditions was observed to follow deadend filtration theory, independent of the shear rate, for short times. For long times, however, the measured fluxes were observed to level out and reach a near steady-state value. This results from the hydrodynamic shear imposed by the crossflow arresting the cake growth. The initial flux and the rate of flux decline for short times were used to determine the membrane resistance and the cake resistance, respectively. The cake resistances for the titania dispersions are considerably higher than those predicted by the Blake–Kozeny equation for laminar flow through incompressible packed beds of monodispersed, rigid spheres. It is likely, that cakes formed under crossflow conditions are more compact that those formed deadend or stagnant conditions. Predicted fluxes show a notable correspondence with experimentally measured values. The model thus gives a basis for estimating the optimal parameters for the design of crossflow microfiltration systems operating on concentrated dispersions.

## Acknowledgements

The authors are grateful to the Tioxide Group, England, for providing the rutile sample, to the Engineering and Physical Sciences Research Council and Tioxide for providing a studentship for JQM, and to The Royal Society Postdoctoral Fellowship Programme which supported one of the authors (PM).

## Appendix A. Nomenclature

| | |
|---|---|
| $a$ | Particle radius (m) |
| $J$ | Permeate flux ($l\,m^{-2}\,h^{-1}$) |
| $J(t)$ | Permeate flux at time $t$ ($l\,m^{-2}\,h^{-1}$) |
| $J_o$ | Pure water flux ($l\,m^{-2}\,h^{-1}$) |
| $J_{SS}$ | Steady-state permeate flux ($l\,m^{-2}\,h^{-1}$) |
| $K$ | Consistency parameter (Pa $s^n$) |
| $n$ | Flow index |
| $\Delta P$ | Transmembrane pressure (Pa) |
| $r$ | Cake layer resistance ($m^{-2}$) |
| $R_m$ | Membrane resistance ($m^{-1}$) |
| $t$ | Time (s) |
| $t_{ss}$ | Time predicted to achieve steady-state (s) |
| $u$ | Inlet crossflow velocity of bulk dispersion ($m\,s^{-1}$) |
| $x$ | Coordinate denoting longitudinal direction of dispersion flow (m) |

*Greek letters*

| | |
|---|---|
| $\delta$ | Cake layer thickness (m) |
| $\gamma$ | Shear rate ($s^{-1}$) |
| $\eta$ | Apparent viscosity (Pa s) |
| $\eta_C$ | Apparent viscosity of the cake layer (Pa s) |
| $\eta_\infty$ | Constant viscosity at the infinite shear limit (Pa s) |
| $\mu_o$ | Dynamic viscosity of pure fluid (Pa s) |
| $\tau$ | Shear stress (Pa) |
| $\tau_C$ | Yield stress in the Casson model (Pa) |
| $\tau_{cr}$ | Time constant (s) |
| $\tau_{HB}$ | Yield stress in the Herschel–Bulkley model (Pa) |
| $\phi$ | Solids volume fraction |
| $\phi_g$ | Gel concentration |
| $\phi_{max}$ | Maximum solids volume fraction in the cake layer |
| $\phi^*$ | Maximum packing density of particles, Eq. (12) |

## References

[1] D.A.R. Jones, B. Leary, D.V. Boger, J. Coll. Interface Sci. 147 (1991) 479–495.
[2] P. Mikulášek, R.J. Wakeman, J.Q. Marchant, Chem. Eng. J. 67 (1997) 97–102.
[3] W.F. Blatt, A. Dravid, A.S. Michaels, L. Nelson, Solute polarization and cake formation in membrane ultrafiltration: causes, consequences and control techniques, in: J.E. Flinn (Ed.), Membrane Science and Technology, Plenum, New York, 1970, pp. 47–97.
[4] F.W. Altena, G. Belfort, Chem. Eng. Sci. 39 (1984) 343–355.
[5] D.A. Drew, J.A. Schonberg, G. Belfort, Chem. Eng. Sci. 46 (1991) 3219–3224.
[6] A.L. Zydney, C.K.A. Colton, Chem. Eng. Commun. 47 (1986) 1–7.
[7] R.H. Davis, D.T. Leighton, Chem. Eng. Sci. 42 (1987) 275–281.
[8] D. Leighton, A. Acrivos, J. Fluid Mech. 181 (1987) 415–430.
[9] C.A. Romero, R.H. Davis, J. Membr. Sci. 39 (1988) 157–185.
[10] R.H. Davis, J.D. Sherwood, Chem. Eng. Sci. 45 (1990) 3203–3209.
[11] C.A. Romero, R.H. Davis, Chem. Eng. Sci. 45 (1990) 13–25.
[12] W.M. Lu, S.C. Ju, Sep. Sci. Technol. 24 (1989) 517–540.
[13] R.H. Davis, Sep. Purif. Meth. 21 (1992) 75–126.
[14] R.H. Davis, Theory for crossflow microfiltration, in: W.S. Winston Ho, K.K. Sirkar (Eds.), Membrane Handbook, Van Nostrand Reinhold, New York, 1992, pp. 480–505.
[15] G. Belfort, R.H. Davis, A.L. Zydney, J. Membr. Sci. 96 (1994) 1–58.
[16] Q.D. Nguyen, D.V. Boger, Annu. Rev. Fluid Mech. 24 (1992) 47–88.
[17] J.Q. Marchant, R.J. Wakeman, Crossflow microfiltration of concentrated titania suspensions, Proc. IChemE Jubilee Research Event, Vol. 2, Nottingham, 1997, p. 1061.
[18] M. Asaadi, D.A. White, Chem. Eng. J. 48 (1992) 11–16.
[19] R.G. Holdich, I.W. Cumming, B. Ismail, Trans. IChemE 73A (1995) 20–26.
[20] R. Rautenbach, G. Schock, J. Membr. Sci. 30 (1988) 231–242.
[21] G. Schulz, S. Ripperger, J. Membr. Sci. 40 (1989) 173–187.
[22] R.J. Wakeman, Trans. IChemE, 72A (1994) 530–540.
[23] E.S. Tarleton, R.J. Wakeman, Trans. IChemE 72A (1994) 431–440.
[24] A.G. Fane, J. Membr. Sci. 20 (1984) 249–259.
[25] G. Akay, R.J. Wakeman, Chem. Eng. Sci. 49 (1994) 271–283.
[26] G. Akay, R.J. Wakeman, J. Membr. Sci. 88 (1994) 177–195.
[27] G. Akay, Z.G. Bhumgara, R.J. Wakeman, Trans. IChemE 73A (1995) 783–796.
[28] R.J. Wakeman, G. Akay, J. Membr. Sci. 106 (1995) 57–65.
[29] R.J. Wakeman, G. Akay, J. Membr. Sci. 91 (1994) 145–152.
[30] R.J. Wakeman, Electrically enhanced microfiltration of albumin suspensions, Trans IChemE (submitted).
[31] R.J. Wakeman, G. Akay, Filtr. Sep. 34 (1997) 511–519.
[32] R.B. Bird, W.E. Steward, E.N. Lightfoot, Transport Phenomena, Wiley, New York, 1960.
[33] R.W. Field, D. Wu, J.A. Howell, B.B. Gupta, J. Membr. Sci. 100 (1995) 259–272.
[34] S. Datta, J.L. Gaddis, Sep. Sci. Technol. 32 (1997) 327–353.
[35] M. Mooney, J. Coll. Sci. 6 (1951) 162–170.
[36] G. Green, G. Belfort, Desalination 35 (1980) 129–147.
[37] R.J. Baker, A.G. Fane, C.J.D. Fell, B.H. Yoo, Desalination 53 (1985) 81–93.
[38] E.S. Tarleton, R.J. Wakeman, Trans. IChemE 71A (1993) 399–410.